Advanced Modeling of Cold Crucible Induction Melting for Process Control and Optimization - 8359

J. A. Roach
Idaho National Laboratory
P. O. Box 1625, Idaho Falls, ID 83415

D. B. Lopukh, A. P. Martynov, B. S. Polevodov, S. I. Chepluk
St. Petersburg Electrotechnical University "LETI"
5 Prof. Popova Str., St. Petersburg, 197376, Russia

ABSTRACT

The Idaho National Laboratory (INL) and the St. Petersburg Electrotechnical University "LETI" (ETU) have collaborated on development and validation of an advanced numerical model of the cold crucible induction melting (CCIM) process. This work was conducted in support of the Department of Energy (DOE) Office of Environmental Management Technology and Engineering (EM-20) International Program. The model predicts quasi-steady state temperature distributions, convection cell configurations, and flow field velocities for a fully established melt of low conductivity non-magnetic materials at high frequency operations. The INL/ETU ANSYS© finite element model is unique in that it has been developed specifically for processing borosilicate glass (BSG) and other glass melts. Specifically, it accounts for the temperature dependency of key material properties, some of which change by orders of magnitude within the temperature ranges experienced (temperature differences of 500°C are common) in CCIM processing of glass, including density, viscosity, thermal conductivity, specific heat, and electrical resistivity. These values, and their responses to temperature changes, are keys to understanding the melt characteristics. Because the model has been validated, it provides the capability to conduct parametric studies to understand operational sensitivities and geometry effects. Additionally, the model can be used to indirectly determine difficult to measure material properties at higher temperatures such as resistivity, thermal conductivity and emissivity. The model can also be used to optimize system design and to predict operational behavior for specific materials and system configurations, allowing automated feedback control. This becomes particularly important when designing melter systems for full-scale industrial applications.

INTRODUCTION

The baseline technology for immobilization of the DOE high level waste (HLW) inventory is vitrification in a BSG using joule-heated ceramic melters (JHCMs). This is a mature and well understood technology; nevertheless, it has several limitations and the DOE continues to invest tens of millions of dollars annually to push the limits of the technology in an attempt to meet the technical and schedule challenges associated with HLW disposition.

The CCIM technology has been identified in numerous studies [1, 2, 3] as a potential alternative to the JHCM technology. It has also been identified by the DOE Office of Nuclear Energy Global Nuclear Energy Partnership program as a potential technology for immobilizing some of the waste streams projected to be generated by advanced fuel cycles [4]. Additionally, DOE-EM recently funded a Phase II project through the Advanced Remediation Technologies program to investigate the feasibility of retrofitting a DOE vitrification facility, such as the Defense Waste Processing Facility (DWPF) at Savannah River Site, with the CCIM technology. However, the CCIM is considered to be less mature than JHCM technologies, at least in the United States, for application to processing of radioactive liquid wastes, and further understanding of the operations parameters, capabilities, and limitations is needed. Recently, interest in the CCIM technology has grown due to the increasingly challenging waste chemistries that are projected to be processed in the DWPF, as well as the planned Waste Treatment Plant (WTP) at the Hanford Site.

The CCIM technology offers several benefits over JHCMs. These include:

- Ability to operate at higher temperatures, thus allowing the application of more durable matrices
- Greater process flexibility (e.g. insensitive to thermal cycling, ability to process refractory-corrosive chemistries, etc.)
- Greater specific throughput
- Higher waste loadings

While some of these advantages are obviously due to the basic operational physics and construction configuration of the CCIM technology (i.e. higher operating temperatures and greater process flexibility), other advantages have only been demonstrated empirically or anecdotally, and the actual physics and mechanisms that produce these characteristics are not well understood, nor is it clear how to predict and control them.

The INL in collaboration with ETU has developed an advanced numerical model of the CCIM steady-state process. Using ANSYS© software, a model has been developed and experimentally validated that predicts temperature distributions, convection cell configurations, and flow field velocities for a fully established melt of low conductivity non-magnetic materials (i.e. BSG, etc.) at high frequency operations (i.e. 0.05 to 30 MHz frequency range).

Extensive modeling of CCIM processes at lower frequencies for metal processing has been conducted, but these models typically provide simplified approaches to account for changes in material properties due to temperature differences within the melt. This is acceptable because the relative changes in the material properties are generally not significant, especially from a model convergence stand point. Additionally, in induction melting of metallic materials, the Lorentz forces dominate the flow regime and buoyancy driven convection cells do not generally form and thus do not significantly contribute to the overall temperature distribution. This is not the case when modeling CCIM processing of BSG and other glass melts.

The INL/ETU ANSYS© finite element model is unique in that it has been developed specifically for processing BSG and other glass melts. Specifically, it accounts for the temperature dependency of key material properties, some of which change by orders of magnitude within the temperature ranges experienced (temperature differences of 500^{o}C are common) in CCIM processing of glass, including density, viscosity, thermal conductivity, specific heat, and electrical resistivity. These values, and their responses to temperature changes, are keys to understanding the melt characteristics. Because the model has been validated, it provides the capability to conduct parametric studies to understand operational sensitivities and geometry effects. Additionally, the model can be used to indirectly determine difficult to measure material properties at higher temperatures, such as resistivity, thermal conductivity and emissivity.

The model can also be used to optimize system design and to predict operational behavior for specific materials and system configurations, allowing automated feedback control. This model has been used to support development of an innovative draining mechanism that can process very high temperature materials (i.e. >1350^{o}C), with no moving parts. The model has also been used to verify bulk temperature and electrical resistivity values for correlation with sensor readings for automated feedback control signals for CCIMs. This paper will discuss the model features and present specific applications where the model is being applied.

MODEL DEVELOPMENT

The commercial finite element modeling software ANSYS MultiPhysics was selected to develop a model that could be used to investigate the coupled thermal and hydrodynamic processes associated with melting of materials using induction energy, with specific focus on BSGs. Significant bodies of work have been developed in empirical design of CCIMs in general [5, 6, 7, 8], as well as in numerical model development of CCIM processes, also know as "skull melting" [9, 10, 11, 12, 13, 14], with Bojarevics, Pericieious, Harding, and Wickins [15, 16, 17] representing the most authoritative work in this area. However, these models are focused on lower frequency processing of conductive materials (i.e. nominally 10 kHz to 100 kHz, for steel, titanium alloys, and other metals). Some work has been devoted to mathematical modeling of CCIM processing of oxides and glasses [18, 19, 20]; however, the model that the INL/ETU has developed is more comprehensive and complex in that it is capable of evaluating melt volumes for high frequency processes, including multiple frequency applications, in the 0.1 to 30 MHz frequency range.

The characteristics of the melting process in a CCIM and the resulting condition of the melt volume is a function of multiple fields and effects that are coupled to produce a quasi-steady state condition. These include electromagnetic, temperature, and hydrodynamic (i.e. convection flow that occurs due to buoyancy) effects, as well as temperature-dependent material properties such as thermal conductivity, electrical resistivity, specific heat, viscosity, and density. These effects are inextricably coupled and interdependent. For example, the temperature field depends on the behaviour of the energy deposition due to the electromagnetic field. However, the characteristics of the electromagnetic field are dependent on the electrical resistivity of the material, and the electrical resistivity is dependent on the temperature of the material. The electrical resistivity can vary by several orders of magnitude within the melt volume due to temperature dependence and the resulting buoyancy effects, thus making convergence challenging in a complex model.

The key to developing a representative numerical model is knowledge of the behaviour of the material properties as a function of temperature. Unfortunately, very little data are available for glass behaviour at temperatures above 1200^{o}C. The material properties used in the model were based on a known glass composition that is referred to as SRL-411 [21]. Farnsworth [21] identifies key material properties for the SRL-411 glass composition at various temperatures up to 1200^{o}C; however, for the ANSYS© model, material properties were needed for higher temperatures. Using these data, as well as information related to the glass chemical composition, the material properties were extrapolated out to 2000^{o}C using the appropriate linear regression techniques that provided reasonable and physically feasible results. Additionally, data were obtained from researchers at Pacific Northwest National Laboratory (PNNL) [22] for electrical resistivity and viscosity values for several glass compositions up to 1500^{o}C. Curve fit equations for these data were developed using Vogel-Fulcher-Tammann, Arrhenius, and other appropriate techniques to define equations that represented experimental data.

For the purposes of this work, the composition of the SRL-411 glass was compared to that of the glasses tested; and the viscosity and resistivity property data were selected for the glass with the nearest composition, based on elemental groupings (i.e. glass forming oxides, alkaline metal oxides, etc.). Table 1 provides a comparison of the SRL-411 glass composition and the actual frit used in the experiments. As indicated in the table, the compositional amounts of elemental groupings are similar. Accordingly, the SRL-411 material property values were accepted for all except the viscosity and resistivity properties.

Additionally, since Vienna [22] had conducted later work on electrical resistivity and viscosity measurements for BSGs at higher temperatures these values were investigated. Analyses of the key components that effect viscosity and electrical resistivity were conducted by comparing the experimental glass composition to that of the "CVS3-1" baseline glass referenced in [22] and determining the overall property effects. The results were shown to align well with the reported values and resulting curve fit

Oxide	SRL-411 (%)	SRNL Experimental Frit (%)
Al_2O_3 (a)	4.7	6.5
B_2O_3 (a)	8.8	7.7
CaO (d)	1.2	1.3
Cr_2O_3 (c)	0.1	0.0
Fe_3O_4 (c)	13.5	10.8
K_2O (b)	2.6	0.0
Li_2O (b)	3.5	4.8
MgO (d)	0.7	0.0
MnO_2 (c)	2.3	1.4
Na_2O (b)	11.5	11.8
NiO (c)	1.1	0.0
SiO_2 (a)	49.0	55.7
TiO_2 (c)	1.0	0.0
TOTAL	100.0	100.0
Elemental Groupings		
Glass Forming Oxides (a)	62.5	69.9
Alkaline Metal Oxides (b)	17.6	16.6
Iron oxide and other oxides with similar properties (c)	18.0	12.2
Modifiers (d)	1.9	1.3
TOTAL	100.0	100.0

Table 1. Comparison of SRL-411 and Experimental Frit Compositions

equations for the electrical resistivity and viscosity of the CVS3-1 glass and thus these values were used in the ANSYS© model.

To facilitate the model calculations, the PNNL values were then extrapolated out to 2000°C using the developed curve fit equations. Some limited sensitivity analyses were conducted using the model to investigate the impacts to the results by varying the material properties within margin-of-error type ranges (i.e. 10% to 15%). These studies indicate that the density seems to have the greatest impact on resulting temperature distribution and hydrodynamics. Figure 1 illustrates example temperature-dependent material property curves used for the current ANSYS© model.

The physical characteristics of the model were based on the test platform that exists at the ETU laboratory facility in St. Petersburg, Russia. These are as follows:

- 60 kW power supply for primary inductor
- 7.5 kW power supply for secondary inductor
- Internal diameter of crucible of 300 mm.
- Height of melt volume in cold crucible up to 200 mm.
- Internal diameter of inductor of 320 mm.
- Height of inductor of 200 mm.
- Number of turns on inductor coil is 3.
- Frequency of primary inductor is 1.76 MHz
- Frequency of secondary inductor is 28 MHz, when used.

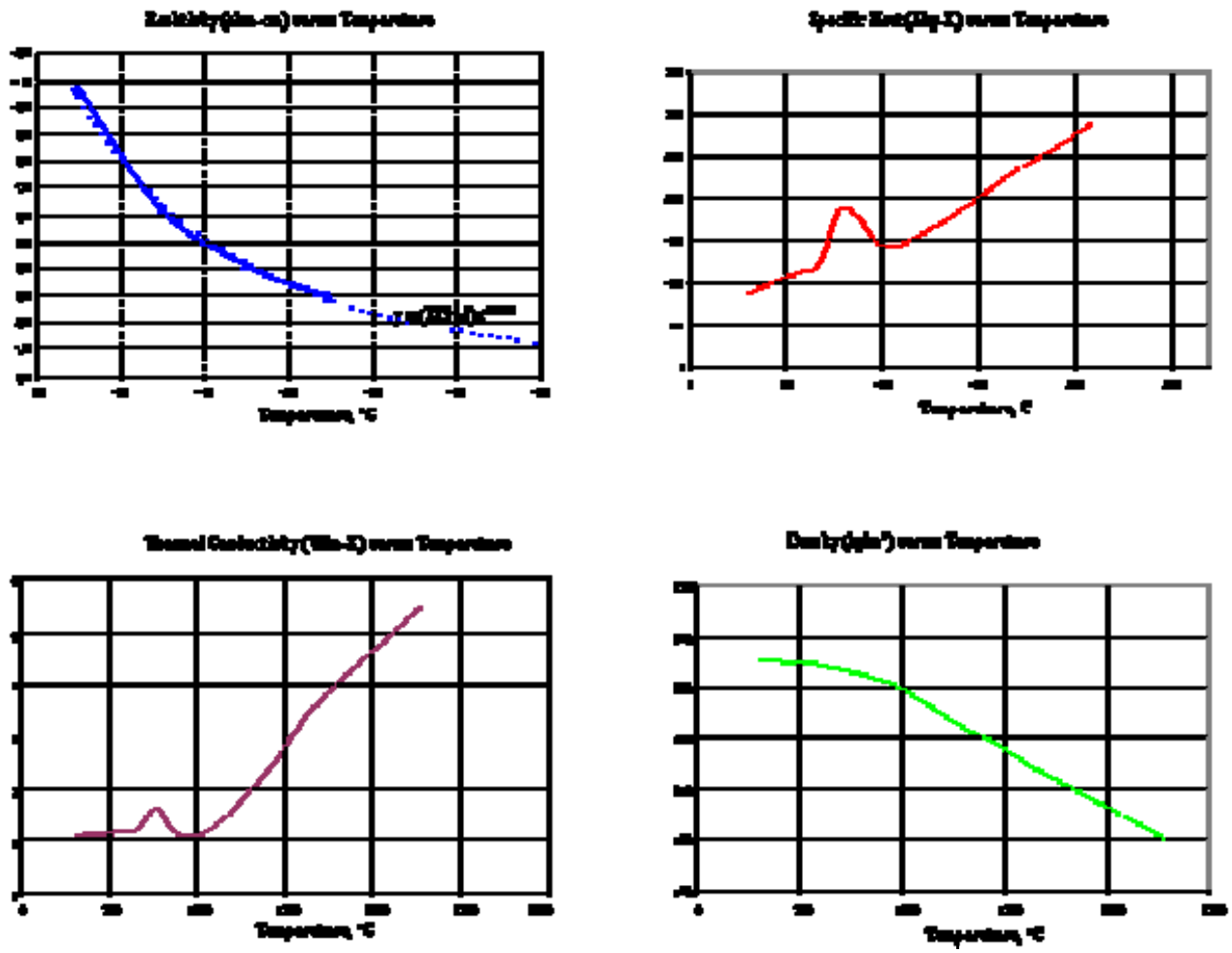

Figure 1. Temperature dependence of material properties of glass

The primary goal of developing the mathematical model was to provide the capability to study the application of an inductively heated high frequency draining device integrated into a CCIM system, which is described in more detail later. The drain device is basically a very small CCIM that is operating at 27 MHz, which is a significantly higher frequency than the primary melter inductor, which is operated at 1.76 MHz. Because both inductors operate at the same time, the ability to investigate the effects of the two frequency integrated melter system was needed.

Accordingly, the CCIM process operations can be considered as two primary steps:

- Glass melting using the primary inductor to achieve a quasi-steady state condition in which the power dissipated in the melt volume, the temperature distribution field, and the melt velocity vector fields stop changing and,
- Melting of the bottom skull within the melter crucible using the secondary drain inductor to initiate melt discharge.

Thus, two mathematical models have been developed for these two stages:

- A model of the quasi-steady state melt conditions using the single frequency primary inductor,

- A model of the non-steady state melting of the bottom skull using both the primary and secondary inductors.

The mathematical model of the quasi-steady state melt achieved using the single frequency primary inductor establishes the conditions of the temperature and melt velocity fields for a given power (i.e. energy deposition) in the melt volume. The current model does not include the effects of the melt initiation process; however, this capability is currently being developed and implemented. The key model parameters and boundary conditions, including power in the melt and heat loss factors (i.e. boundary conditions of the third type for energy flux per unit area and heat radiation conditions), were determined based on experimental calorimetry data. The steady state condition is basically the extreme condition or end state of the non-steady melting process. As such, a time step is established as the iteration parameter in the model. The total heat sources in the melt are calculated every few hundred seconds since this value changes as a function of the melt resistivity, which is temperature dependent. This iterative process continues until the changes in the temperature, velocity, and pressure fields are less than the predetermined convergence values. In addition, at the steady state condition, the total of the calculated power losses must equal the power level supplied to the melt.

The mathematical model of the non-steady state bottom skull melting process uses a two-frequency system. Because it is not steady state, an assumed power level supplied to the melt is not appropriate since it is constantly changing. Alternatively, a value for the current in the small inductor is assumed based on experimental results. On the drain wall a boundary condition of the third kind is defined, and on the drain opening a heat radiation condition is set. Earlier versions neglected this heat loss at the drain opening due to their relatively small values, but this boundary condition was later included. The initial conditions for this model are the electrical, thermal, and hydrodynamic field calculation results obtained from the steady state melt model. Since this process is not steady state, the time increments used for iteration are much smaller than the quasi-steady state block calculation.

The two mathematical models are carried through to convergence through the combined use of the following calculation blocks:

- Electromagnetic calculation block for steady state analyses that allow for setting the power supplied to the melt
- Electromagnetic calculation block for non-steady state analyses that require setting the inductor power (i.e. current in the inductor with known material resistivity and geometry)
- Coupled thermal and hydrodynamic calculation block for melt velocities due to natural convection (i.e. buoyancy effects due to temperature dependent density).

The electromagnetic calculation blocks are based on Maxwell's equations for a quasi-steady state condition, which allows displacement currents in the busses and melt to be neglected. For the present case, the model is represented by the following equations:

$$\nabla \times \vec{H} = \vec{J} \qquad \text{(Eq. 1)}$$

$$\nabla \times \vec{E} = -\frac{\partial \vec{B}}{\partial t} \qquad \text{(Eq. 2)}$$

$$\nabla \vec{B} = 0 \qquad \text{(Eq. 3)}$$

$$\nabla \vec{J} = 0 \qquad \text{(Eq. 4)}$$

$$\vec{J} = \sigma_e \left(\vec{E} + \vec{E}_e \right) \qquad \text{(Eq. 5)}$$

$$\vec{B} = \mu_a \vec{H} \qquad \text{(Eq. 6)}$$

Where:

$\vec{H}$ = magnetic flux density

$\vec{J}$ = conduction current density

$\vec{E}$ = turbulent component of the electric field intensity (specified by the variable magnetic flow)

$\vec{B}$ = magnetic field induction

μ_a = total magnetic permeability of the melt

E_e = external component of the electric field intensity

σ_e = electrical conductivity of the melt

As can be seen in Eq. 5, the conduction current flows are determined by the external and turbulent components of the electrical field. The external component represents an external impact or energy input into the system. In the case of a CCIM system, this is the inductor voltage.

In the mathematical model, for solving Eq. 1 through Eq. 6, the electromagnetic oscillations were assumed to be sinusoidal to simplify the calculations. (Note that the actual signals are very close to sinusoidal but are not pure.) Further model simplifications can be made due to the cylindrical geometry of the CCIM test platform that is used. Accordingly, axial symmetry can be assumed and thus all of the fields (i.e. thermal, electrical, and hydrodynamic) are considered as spatially bivariate. That is, they are only dependent on radial and axial coordinates (i.e. r and z in a cylindrical coordinate system).

Equations 1 through 6 are solved iteratively using the ANSYS finite element model in terms of the vector potential $\vec{A}$, which is specified as:

$$\vec{B} = \nabla \times \vec{A} \qquad \text{(Eq. 7)}$$

$$\nabla \vec{A} = 0 \qquad \text{(Eq. 8)}$$

For a cylindrical system, the vector potential $\vec{A}$ only has a component along the Θ direction, which is a function of *r* and *z*. Thus, a zero value for $\vec{A}$ can be used as the initial condition. Additionally, $\vec{A} = 0$ can be used as the boundary conditions along the axis of symmetry and at the borders of the analysis area. The borders of the analysis bound the calculation area and the model mesh. This boundary is defined by a rule of thumb that has been established and demonstrated to provide accurate results if set at 2 to 3 times the radius of the inductor coil. As previously stated, two separate electromagnetic calculation blocks are used, depending on whether a power level into the melt or current density in the inductor can be set (i.e. steady state or non-steady state).

The calculation block used to determine the hydrodynamic and thermal distribution is based on simultaneously solving the hydrodynamic and energy equations in cylindrical coordinates. These are described as follows:

Continuity:

$$\frac{1}{r}\frac{\partial}{\partial r}(\rho r u_r) + \frac{\partial}{\partial z}(\rho u_z) = 0 \qquad \text{(Eq. 9)}$$

R – Momentum:

$$\rho\left(\frac{\partial u_r}{\partial t}+u_r\frac{\partial u_r}{\partial r}+u_z\frac{\partial u_r}{\partial z}\right)=\frac{1}{r}\frac{\partial}{\partial r}\left(r\sigma_{rr}\right)-\frac{1}{r}\sigma_{\theta\theta}+\frac{\partial\sigma_{rz}}{\partial z}+f_{er} \qquad \text{(Eq. 10)}$$

Z – Momentum:

$$\rho\left(\frac{\partial u_z}{\partial t}+u_r\frac{\partial u_z}{\partial r}+u_z\frac{\partial u_z}{\partial z}\right)=\frac{1}{r}\frac{\partial}{\partial r}\left(r\sigma_{rz}\right)-\frac{1}{r}\sigma_{\theta\theta}+\rho g+f_{ez} \qquad \text{(Eq. 11)}$$

Energy:

$$\rho c_p\left(\frac{\partial T}{\partial t}+u_r\frac{\partial T}{\partial r}+u_z\frac{\partial T}{\partial z}\right)=k\left(\frac{\partial^2 T}{\partial r^2}+\frac{\partial^2 T}{\partial z^2}+\frac{1}{r}\frac{\partial T}{\partial r}\right)+Q_e \qquad \text{(Eq. 12)}$$

Where:

Stresses in the momentum equations are defined as:

$$\sigma_{rr}=-p+2\mu\frac{\partial u_r}{\partial r} \qquad \sigma_{\theta\theta}=-p+2\mu\frac{u_r}{r} \qquad \text{(Eq. 13 and Eq. 14)}$$

$$\sigma_{rz}=\mu\left(\frac{\partial u_r}{\partial z}+\frac{\partial u_z}{\partial r}\right) \qquad \sigma_{zz}=-p+2\mu\frac{\partial u_z}{\partial z} \qquad \text{(Eq. 15 and Eq. 16)}$$

Frequency induced electromagnetic force densities are defined as:

$f_e=\vec{j}\times\vec{H}$, in the r and z directions (Eq. 17)

And

u = velocity components in r and z directions

$\vec{j}$ = frequency induced electric current density

ρ = density

c_p = specific heat

p = pressure

μ = dynamic viscosity

k = thermal conductivity

f_e = frequency induced electromagnetic force density

Q_e = frequency induced heat generation density

Note that all of the material properties are defined in the model as temperature dependent values, including density, specific heat, viscosity, thermal conductivity, and electrical conductivity.

For solution of the energy equation, boundary conditions of the third type are established for the crucible walls and bottom surfaces and the drain walls. The melt surface on the top of the crucible and the bottom of the drain are radiation boundary conditions. These values, including heat transfer per unit area and emissivity have been determined from experimental results through calorimetry. Additionally, these parameters are dependent on the specific configuration of the test system used to conduct validation experiments. Heat fluxes at surface boundaries are functions of the material properties and the convection heat transfer characteristics (i.e. cooling medium, flow velocity, flow path configuration, etc.). Additionally, the ANSYS© software has post-processing capabilities that provides the ability to determine

the heat flux values through specific surfaces, thus allowing validation of the experimental values, as well as determination of the bulk heat transfer coefficient for a specific surface. The boundary conditions of the third type are related to the equation:

$$q'' = h(T_s - T_\infty) \qquad \text{(Eq. 18)}$$

Where:
q'' = heat flux
h = heat transfer coefficient
T_s = surface temperature
T_∞ = temperature of the surrounding environment

For the system described above, the following specific heat transfer parameters were defined, which were determined in numerous tests:

- Thermal flux through the side of the melt pool of 13 W/cm^2
- Thermal flux through the bottom of the melt pool of 1 W/cm^2
- Thermal flux from the top surface of the melt pool due to radiation
- Thermal flux through the side of the melt pool in the drain body of 27 W/cm^2
- Thermal flux from the surface of the melt pool in the bottom of the drain of 1 W/cm^2

For the hydrodynamic calculation, boundary conditions related to the velocity are also defined:

- On the melt surface the normal velocity component equals zero.
- On the side and bottom surfaces of the crucible the normal and tangential velocity components equal zero.
- On the central axis the normal velocity component equals zero.

The electrical block is first executed to establish an initial temperature distribution. This result becomes the input to the block of energy and momentum equations, which then incorporates the effects of the hydrodynamic calculations. This is an iterative calculation that proceeds until the pre-defined convergence criteria for the various parameters are satisfied. The key convergence criteria for Eq. 9 through Eq. 12 are the node pressure values. Melt movement, or convection cell formation, occurs due to natural free convection resulting from the temperature dependent density differences within the melt volume.

The complexity of the coupled models was systematically increased. The initial version did not account for the temperature dependence of the material properties, but used fixed values to simplify initial calculations and ensure functionality of the models. The next version accounted for the temperature-dependence of the material properties. Finally, the electromagnetic block was modified and the geometry of the model to investigate the induction drain device. Once the model included the key parameters needed to function as a useful research tool, it required validation.

MODEL RESULTS AND VALIDATION

The ANSYS© model developed to investigate CCIM operation was originally focused on supporting research of an innovative draining device. Once a functioning model was developed, it was run for various material properties and parameters and the results compared with experimental work for

qualitative representativeness. During this process, the model was readily shown to provide results that were similar to experimental observations and was determined to provide a reliable tool for evaluation of the effects of various design parameters, including material properties and geometry. The following presents a synopsis of this process and the overall results.

The ANSYS© plots shown in Figure 2 illustrate the model results for thermal distribution and radial x-component and axial y-component melt velocities due to buoyancy effects. The upper two plots show temperature distributions in the melt for two CCIM configurations – the top right plot is for a CCIM with a second high frequency (i.e. 28 MHz) induction energy source in the bottom center. While the maximum temperature does not change significantly, note the increase in melt volume that is at the higher

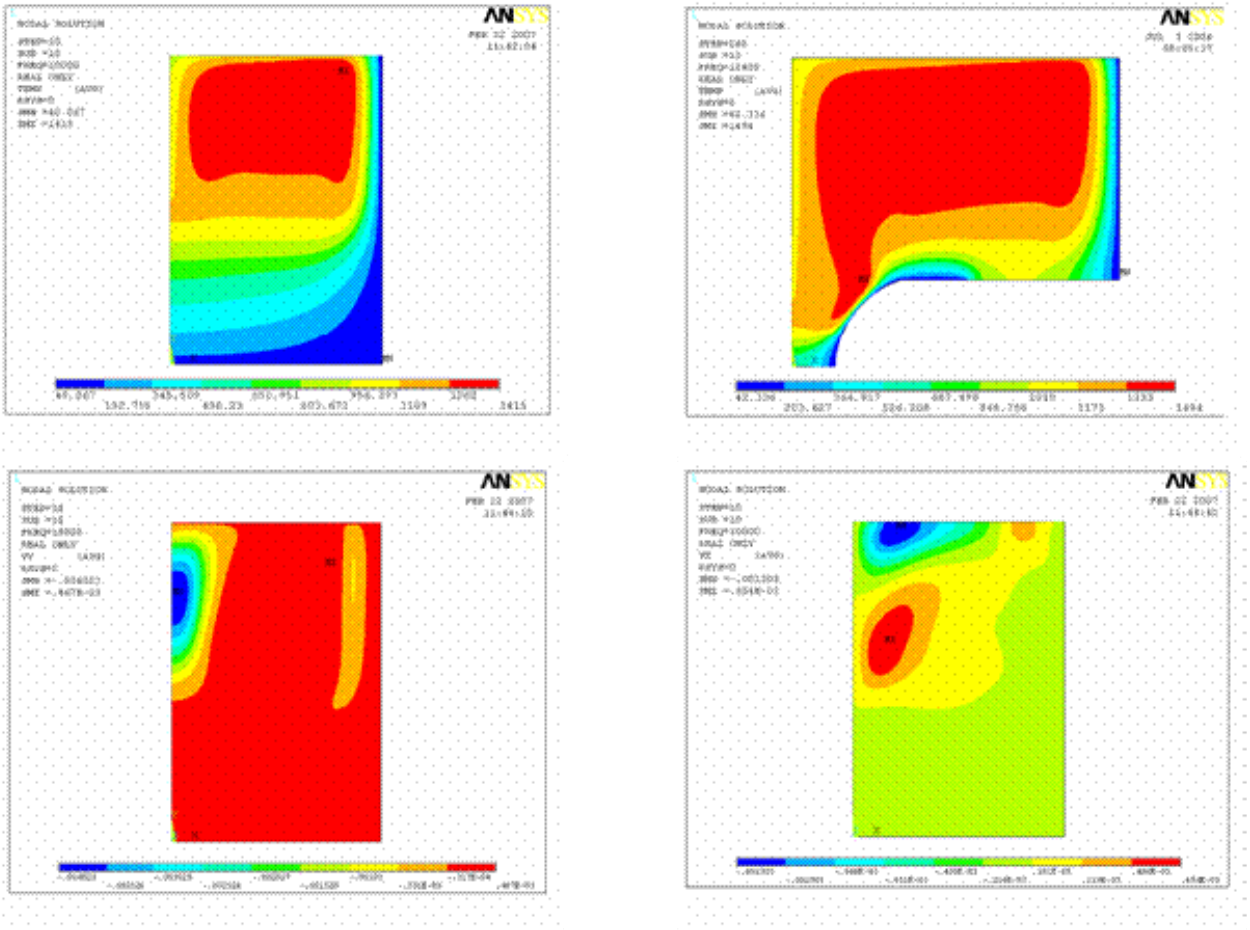

Figure 2. Modeling results of the ANSYS© model for various CCIM configurations.

temperatures, and the overall improvement in thermal homogeneity. The lower two plots show the V_x and V_y velocities for a simple CCIM configuration. The values correlate to an average bulk velocity of about 1 m/hr. As an example, for a 300 mm diameter CCIM, the majority of the glass volume would have been moved throughout the entire volume of the crucible in an hour. Actual measurements in the melter are extremely challenging and costly. The ability to reliably determine these characteristics using the model is a significant benefit. Another interesting phenomenon was observed using the model to investigate temperature distributions related to the aspect ratio between the melt diameter and height, particularly near the bottom. The location of the "hot spot" at the bottom migrates and can thus be controlled and/or used as a key design parameter depending on the system.

The most direct method to determine if the model is providing both quantitative and qualitative results is through measurement of the melt volume temperature profile and comparing this with the model results. For this to be a valid comparison, the model parameters for geometry, glass properties, and operational conditions must be consistent. To accomplish this, an experiment was conducted using a 300 mm diameter CCIM, with a three-turn coil operating at 1.76 MHz, with a 200 mm deep melt bath. An array of thermocouples was constructed such that the thermocouples could be lowered and raised through the melt volume to measure the temperature throughout the melt. A fixed location was identified on the surface of the melt and the temperature measured using an optical pyrometer, and then compared to previous model results to establish consistency in the experimental parameters. The results of this experiment are shown in the graphs in Figure 3, which illustrate outstanding correlation with the model results. Starting at the top right, the plots are for the centerline, and 35, 70, 105, and 122.5 mm from the central axis. The final picture included in this figure is the actual test configuration showing the crucible size and coil configuration.

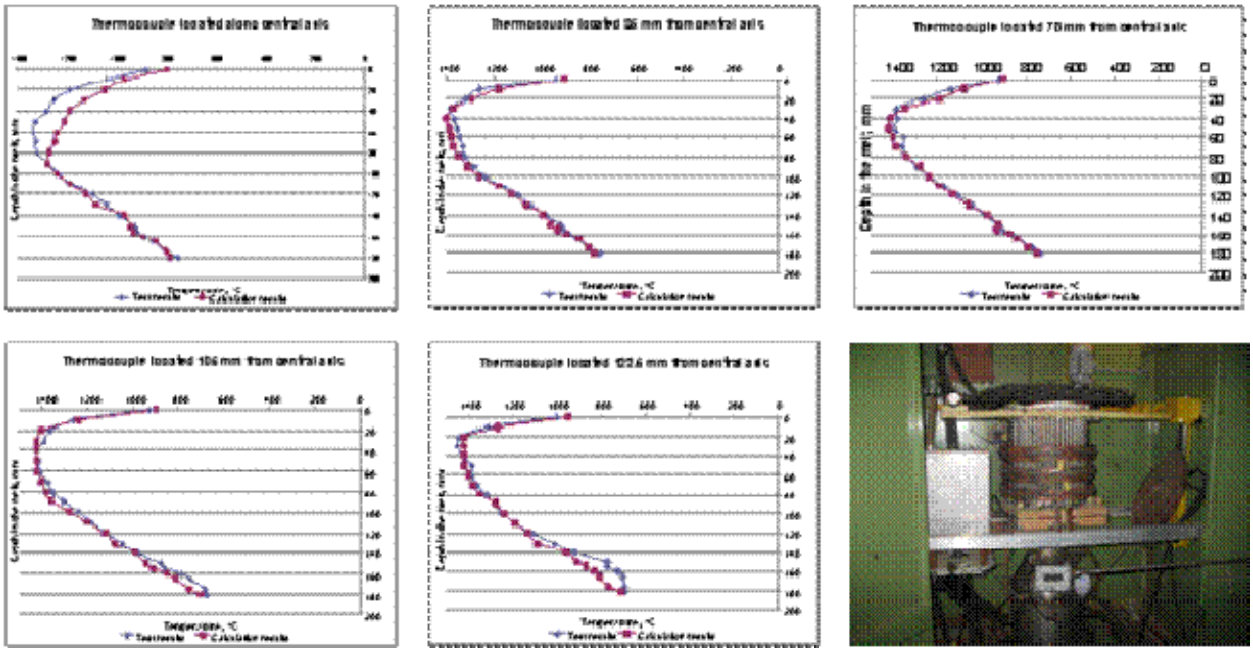

Figure 3. Comparison of modeling and experimental results for temperature distribution, with photo of the test setup

On average, the differences between the experimental and model results are less than 5%. The areas located close to the melt pool axis and the bottom are exceptions. These differences are due to several factors, some of which can be easily addressed, others cannot be. The location of greatest discrepancy occurs on the centerline. This is due to the fact that the model assumes axial symmetry. However, due to the complexity of the dynamically changing inter-related variables, this is not a precise representation of the actual melt volume characteristics. Additionally, effects of bubble formation, temperature fluctuation, shunt currents between the melt and crucible sections, and crystallization in the melt over time are examples of perturbations that are characteristic of this complicated physical process. These factors cannot be accounted for with the current model.

For example, near the perimeter (at 122.5 mm) bottom, significant deviation occurs from the experimental results near 18%. The model indicates higher temperatures than measured during the testing. This is suspected to be a measurement error due to the mechanical force that is applied to the thermocouple as it is lowered into the melt. Because the thermocouples were long and slender, the melt quite likely

deflected the thermocouple such that the measurement was actually farther from the outside wall than indicated. The other potential cause is that the glass properties assumed near 800°C in the model may not accurate. This seems unlikely since these properties are within the range of temperatures for which actual measured data were available. Further investigation and overall refinement of the model will continue.

MODEL APPLICATION

As the ANSYS© model was refined and advanced to include the dual frequency capability, it was used as a research tool to help develop and demonstrate an innovative drain device that uses high frequency induction energy to accomplish a non-mechanical glass casting process. The system developed and tested has been demonstrated to effectively conduct multiple casting operations, accomplishing both initiation and cessation of draining the glass, with no mechanical moving parts (i.e. slides, plungers, plugs, etc.). The utility of the model proved invaluable in conducting investigation of various configurations for efficiency and feasibility. This was particularly due to the high frequency needed for this application. Recall that researchers have determined empirically [7] that for cylindrical melters the diameter should be approximately a factor of 3.8 times the skin depth (represented as δ) at the nominal frequency of operation. The skin depth in centimeters is calculated:

$$\delta = 5 \times 10^3 \left(\frac{\rho}{\mu f} \right)^{1/2} \qquad \text{(Eq. 19)}$$

Accounting for the 3.8 factor and rearranging, the optimal frequency of operation can be determined with:

$$f = 3.6 \times 10^8 \left(\frac{\rho}{\mu d^2} \right) \qquad \text{(Eq. 20)}$$

Where:
δ = skin depth
f = frequency
d = diameter

For the range of diameters that would effectively function as a drain for processing glasses, this correlates to a frequency in the range of 25 MHz to 30MHz.

The interaction of the multiple variables associated with an induction melting process is quite complex and extremely challenging to investigate analytically. Typically, significant experimentation is required, which can be costly and time consuming. The ANSYS© model that INL/ETU have developed was valuable in helping to focus the experimental efforts, such they were bounded and typically were validation experiments rather than exploratory. Specifically, the model was effectively used to determine the power requirements for the drain, the temperature necessary in the region above the drain to initiate downward melt propagation, the drain geometry, including diameter, length, and radius, and the location and number of turns needed on the drain inductor. The result is that this drain device has now been designed, constructed, implemented into a CCIM system, and validated. Figure 4 shows modeling and experimental results that illustrate the use of the ANSYS© model to help successfully design, construct, and validate an innovative technology. Further work is needed to continue to refine and improve the operation of the drain device, which will be greatly enhanced through use of the INL/ETU model.

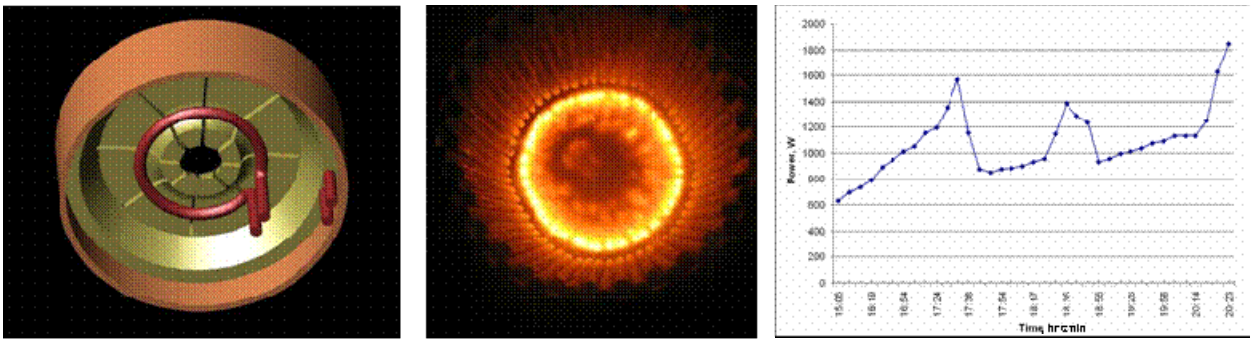

Figure 4. Model of an innovative induction drain device, photo of melt surface just prior to opening drain, and data plot of energy in the drain at each of three consecutive draining events.

Similar models could be developed for other systems, taking into account specific parameters and geometries, now that the basic structure has been developed and validated.

CONCLUSIONS AND FUTURE WORK

The INL and ETU have collaborated on development and validation of a unique numerical model using the ANSYS© MultiPhysics platform for application to induction melting of non-conductive materials requiring very high frequencies. The experimental results presented in this paper demonstrate that the model provides data that are very representative of actual experimental results. Consequently, this model can now be reliably used to conduct investigations of a wide variety of CCIM-based systems. The numerical structure has been defined and validated such that modification of the model to investigate many types of systems is quite feasible.

However, to fully understand the application and utility of the model several enhancements and investigations are needed. For example, continued investigation of geometry effects and how to optimize them for various applications is needed. Key to these types of investigations is the need to understand the sensitivity of the model results to the parameters provided. Specifically, sensitivity studies are needed to determine if the model responds in a quantifiable manner to changes in temperature-dependent material properties such that one could work backwards to actually define unknown and/or difficult to measure properties, such as resistivity and thermal conductivity. Likewise, understanding if a simplified model is acceptable, or if a more complex model is needed to achieve representative results, is very important. For example, is the development of a 3D model needed such that the axial symmetry assumption is not invoked, thus eliminating some of the current inconsistencies between calculation and experimental results. These are the types of investigations necessary to optimize the model utility and accuracy.

Finally, as described above, the INL/ETU model is primarily a steady-state model. Follow-on work to model and better understand the transient processes associated with CCIM operations would be significantly beneficial. Future efforts should be focused on enhancing the model to include these transient phases, including melt start-up, draining with various phenomenon, and re-start. Start-up of induction melting of BSG is an interesting process because at low temperatures the glass is virtually non-conductive; then, at elevated temperatures the glass becomes conductive, relative to the initial condition. The electrical conductivity changes by several orders of magnitude between room temperature and CCIM operational temperatures. The process typically involves introduction of a conductive material to couple with the induction energy field. As this material is super-heated the surrounding glass is melted due to thermal conduction. As this melt pool increases, the induction field couples more with the melt and the voltage and current on the generator lamp anode changes. Currently this is simulated for steady state by fixing the power in the melt, which has been experimentally determined, and iterating through a loop to determine the current, based on the electrical conductivity value of the glass, which changes significantly with temperature. Development of a mathematical model in which the inductor voltage can be defined

rather than power in the melt is of great interest. This enhancement would provide the capability to model the melt start-up process. Similar benefits could be gained from modeling the draining process and understanding the effects on operation, time constant for re-establishing steady state, operational constraints, thus being able to optimize the overall process.

The most important feature of the INL/ETU model is that it provides the capability to calculate temperature distribution and convection cell characteristics in large high-efficiency industrial scale melters. As the melter diameter increases, the inductor current frequency must also decrease to maintain electrical efficiency. Thus, the processes and characteristics of heat transfer and melt flow change considerably, which drives the design and configuration. Application of this model to the design of large melters with different geometries and configurations would allow cost-effective and expeditious evaluation, optimization, and design selection.

REFERENCES

1. J. M. Perez et al., "High-Level Waste Melter Study Report", PNNL-13582, July 2001.
2. J. Ahearne et al., "High-Level Waste Melter Review Report", TFA-0108, July 2001.
3. R. L. Treat et al., "Technical Evaluation of Hanford HLW Vitrification Process Alternatives: Report of the Independent Project Evaluation Team", July 2003.
4. D. Gombert III, et al., "Global Nuclear Energy Partnership Integrated Waste Management Strategy Waste Treatment Baseline Study", GNEP-WAST-WAST-AI-RT-2007-000324, September 2007.
5. J. F. Wenckus, et. al., "Study, Design and Fabricate a Cold Crucible System," Air Force Cambridge Research Laboratories, March 31, 1975, AFCRL-TR-75-0213.
6. P. G. Clites, "The Inductoslag Melting Process", *Bulletin 673*, U.S. Department of the Interior, 1982.
7. D. Venable and T. P. Kim, "Radio Frequency Heating Fundamentals and Applications," Westinghouse Electric Corporation, 1946, p. 379.
8. D. Lopukh, "Process Research and Development of Equipment for Solidification of Radioactive Waste Simulators by Induction Cold Crucible Melting," Leningrad Electrotechnical Institute, September 2003.
9. Wan-Soo Kim and Jong-Kyu Yoon, "Numerical Prediction of Electromagnetically Driven Flow in ASEA-SKF Ladle Refining by Straight Induction Stirrer," *Iron and Steel Making, 1991, Vol. 18, No. 6,* pp. 446 – 453.
10. Pil-Ryung Cha, et. al., "Numerical Analysis on Cold Crucible Using 3D H-Φ Method and Finite Volume Method with Non-staggered BFC Grid System," *Iron and Steel Institute of Japan International, Vol. 36, 1996, No. 9*, pp 1157 – 1165.
11. V. Clingoski, Hideo Yamashita, "Analysis of Induction Skull Melting Furnace by Edge Finite Element Method Excited from Voltage Source", *IEEE Transactions on Magnetics, Vol. 30, No. 5, September 1994*
12. Yanquing S, et al, "Modeling of Temperature Field for Induction Skull Melting Process of Ti-47Ni-9Nb", *Metallurgical and Materials Transactions A, Vol. 32A, November 2001*, pp. 2895-2902.
13. Y. Su, S. Guo, G. Liu, J. Jia, H. Ding, "Temperature Control of TiAl Melt During Induction Skull Melting", *Materials Science and Technology, Nov 2001, Vol. 17 (ISSN 0267-0836)*, pp. 1434-1440.
14. J. Gue, G. Liu, Y. Su, H. Ding, J. Jia, H. Pu, "Skull Variation During Induction Skull Melting Processing of Gamma-TiAl Alloy", *Materials Science and Technology, Vols. 475-479 (2005)*, pp. 809-812.
15. V. Bejarevics, K. Pericieious, R. Harding, M. Wickins, "Induction Skull-Melting Dynamics for Different Materials: Numerical Modeling and Comparison with Experiments:, *Modeling of Casting, Welding, and Advanced Solidification Processes X, 2003*, pp. 591-598.
16. V. Bejarevics, K. Pericieious, R. Harding, M. Wickins, "The Development and Experimental Validation of an Induction Skull Melting Furnace", *Metallurgical and Material Transactions B, Vol. 35B, August 2004*, pp. 785-803.

17. V. Bejarevics, K. Pericieious, R. Harding, M. Wickins, "Experimental and Numerical Study of the Cold Crucible Melting Process", *Third International Conference on CFD in the Materials and Process Industry, CSIRO, December 2003*, pp. 599-606.
18. A. Lubomirov, D. Lopukh, et al, "Features of Induction Melting of Oxides in a Cold Crucible", *Electrometallurgia Journal, No. 2, 2002*, pp. 32-36.
19. Yu. Petrov, D. Lopukh, A. Pechenkov, "Continuous Glass Melting in Induction Furnace with Cold Crucible, *International Congress on Glass Proceedings, Vol 3a, Nauka, Leningrad 1989*, Edited by O. V. Mazurin.
20. B.. S. Polevodov, "Mathematical Models of Induction Melting in Cold Crucibles", *Electrical Technology, Russia, No. 3, 2002*.
21. R. K. Farnsworth, et al, "Applications of TEMPEST Computer Code to Canister-Filling Heat Transfer Problems", PNL-6474, March 1988.
22. J. D. Vienna, et al, "Effect of Composition and Temperature on the Properties of High-Level Waste (HLW) Glass Melting Above 1200^{o}C" (DRAFT), PNNL-10987 UC-810, April 1996.